The Design, Analysis and Fabrication of a Six-Axis Micropositioning Stage

Kao-Hui Lin and Ya-Hui Hu

Abstract—**Micro/nano positioning stages play an essential role in micro/nano precision technology, so the design and development of a new six-axis micro positioning stage are presented in this research. Based on Steward's theory, the stage adopts negative Poisson's ratio with flexure hinges. Since each of the axes is a planar mechanism structure, the stage is fabricated out of aluminum with the micro machining - a simple and well - developed fabrication technique for cost down and batch production. The stage consists of a top plate and a base plate, two hexagons of which the diameters are respectively 22 mm and 95.2 mm with a distance of 21.6 mm in between, and six trapezoid amplifiers, each of which is connected to the base plate at an angle of 30°. Each amplifier consists of three layers – two inner layers of symmetrical flexure hinges and one outer layer of non-symmetrical flexure hinge.**

In this research, the stress, strain and amplification are calculated with the software of SolidWorks Ansys@. In experiment, each amplifier is driven by a piezoelectric transducer (PZT), and the displacements are measured with a laser displacement sensor and recorded for comparison of the single-axis amplifier with the six-axis stage. The results show that the amplification of the displacement of a single-axis amplifier is 15 times, that the horizon translation, the vertical translation, the tilt angle and the rotational angle are 50 μm, 50 μm, 0.5° and 0.5° respectively, and that the displacement resolution and the rotational resolution are 15.6 nm and 2.7 μrad respectively. It is obvious that the six-axis stage of this research, indeed, retains the features of high amplification and minimization, and is a novel and low-cost six-axis micropositioning stage.

Index Terms—**Six-axis Micropositioning Stages, Negative Poisson's Ratio, Flexure Hinge, Steward's Stage.**

I. INTRODUCTION

Along with the progress in industry technology, the development of micro/nano technology has become of great interest to precision technology, especially in fields like electron, communication, assembly, testing, and so on. However, it is hard to develop micro/nano technology through traditional series servo systems. Therefore, the design of a nano mechanism of high speed moving, high resolution and long travel as well as the adoption of a suitable actuator will definitely improve the precision of the stage.

Positioning stages, which play the role of loading and positioning an object, are generally expected to maintain a certain degree of stability so as to avoid making any noise in

K. H. Lin is with the Department of Mechanical Engineering, Ching Yun University Chung Li, Taiwan 320 (e-mail: khlin@cyu.edu.tw)
Y. H. Hu is with the Department of Mechanical Engineering, Nanya Institute of Technology Chung Li, Taiwan 320 (She is corresponding author, fax: 886-3-4384670, e-mail: yahuihu@nanya.edu.tw).

vibration. The stages also need to retain certain features such as high precision, long travel, mutil-DOF and high wideband control. In the application of micro/nano technology, the PZT, a device of small size, high resolution and high precision [1], is now the most frequently used device in the positioning system. However, since its motion range is very small, it cannot satisfy the requirement for long travel in many cases [2].

According to the literatures in the past decades, the ways to design precise positioning stages are roughly categorized as follows. One way is based on the multi-linkage mechanism theory, which is to make the stage move on an $XY\theta$ stage, with a device that connects a bar to a joint [3], such as a two-axis flexure hinge, or to make the stage move in 2-DOF, with a four-bar flexure parallel mechanism [4] to control the movement of the stage. In 2006, Chu [5] and his group, using a flexure hinge and a parallel elastic mechanism, succeeded in making a novel long-travel piezoelectric- driven linear nanopositioning - 50 μm in moving range and 10 nm in resolution. Another way is based on the kinematics theory, which is to use the magnetic field effect engendered by four sets of coils and four sets of magnets to control the kinematical motion – 100 mm in XY moving range, 200 nm in linear resolution, and 0.2" in rotational resolution.

No matter how many documents or records have shown efforts in designing and developing micropositioning stages, most of them are confined only to the development of planar motion stages integrated with $XY\theta$. In this research, a six-axis micropositioning stage with 6-DOF is being designed and fabricated, based on Stewart's theory of "A Platform with Six Degrees-of-Freedom" [7]. The concept of this design is derived from the material traits of the negative Poisson's ratio [8] and the flexure hinge mechanism [9], trying to make a six-axis mechanism of negative Poisson's ratio with flexure hinges [10]. It is a parallel mechanism of high stiffness, which can offer 6 degrees of freedom, with its size controlled under 100 mm x 100 mm x 30 mm, its linear resolution at 15.6 nm, and its rotational resolution at 2.7 μrad. Constructed with six parallel single-axis amplifiers, the stage does not add up the error from each single-axis amplifier and, therefore, is able to satisfy the requirement for high precision. Besides, with each of its amplifiers consisting of three layers – two inner layers of symmetrical flexure hinges and one outer layer of non-symmetrical flexure hinge [11], when actuated by the PZT, the stage can be used as a micro displacement stage of high precision. Finally, with the help of a commercial software package (**SolidWorks Ansys**[@]), we get to analyze kinematics and measure deformations based on the finite elements [12], and to calculate the amplification in numerical simulation and experiment. By comparing the

deformation of numerical solutions, analytical solutions and experiment results in the algorithm of the six-axis stage, this research demonstrates the precision of the stage.

II. THE DESIGN OF THE SIX-AXIS STAGE

As shown in Fig. 1, the six-axis stage designed in this research, with six PZT actuators driving the mechanism of negative Poisson's ratio with flexure hinges, can generate a force to push all of the six amplifiers toward the center, minimize the gaps between the PZT actuators and the amplifiers, promote the precision of the mechanism and expand its displacement. It consists of a top plate (a hexagon of 22 mm in diameter and 3mm in height), a base plate (a hexagon of 95.2 mm in diameter and 3 mm in height), and six piezoelectric-driven displacement amplifiers which, respectively symmetrical to either of their neighboring ones, are all connected to the edges of the top and the base plates and meet the base one at an angle of 30º. The distance between the top plate and the base plate is 21.6 mm. Each of the amplifiers, as shown in Fig. 2, is a trapezoid, of which the shorter parallel side connected to the top plate is 12 mm, the longer parallel side connected to the base plate is 56 mm, the height is 44 mm and the thickness is 3 mm. Since each of the amplifiers consists of three layers – two inner layers of symmetrical flexure hinges and one outer layer of non-symmetrical flexure hinge, the three-layered amplifier mechanism can not only enlarge the amplification and enhance the spatial utilization ratio, but also minimize its frame size so as to achieve high amplification.
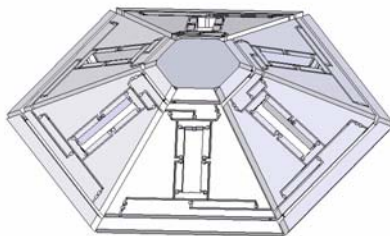
Fig. 1 Six-Axis stage
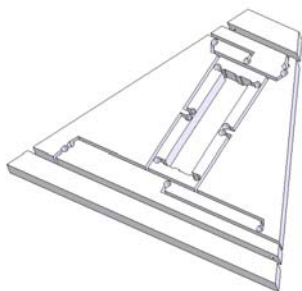
Fig. 2 A single amplifier

III. THE ALGORITHM OF THE SIX-AXIS STAGE

In this paper, the motion of the six-axis stage is discussed based on the global coordinate system (as shown in Fig.3). The system adopts two local coordinate frames: a base frame B and a plate coordinate frame P. Frame P consists of six

connection points ($P_i = \begin{bmatrix} P_{ix} & P_{iy} & P_{iz} \end{bmatrix}$ for i = 1 ~ 6) that join the amplifiers to the top plate, whereas Frame B consists of six other connection points ($B_j = \begin{bmatrix} B_{jx} & B_{jy} & B_{jz} \end{bmatrix}$ for j = 1 ~ 6) that join the amplifiers to the base plate. We use three translations and three rotations to make (x, y, z, α, β, γ) to indicate the relativity vector V of each point to Frame P and Frame B. Thus, we get the rotation matrix R as shown in Algorithm (1), where C = cos, S = sin, and the matrix {P} is included in $\begin{bmatrix} V \end{bmatrix}$.
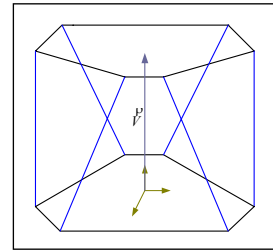
Fig. 3 A schematic diagram of the measurement global coordinate system.

$$R = R_X R_Y R_Z$$
$$= \begin{bmatrix} 1 & 0 & 0 \\ 0 & c_\alpha & s_\alpha \\ 0 & -s_\alpha & c_\alpha \end{bmatrix} \begin{bmatrix} c_\beta & 0 & -s_\beta \\ 0 & 1 & 0 \\ s_\beta & 0 & c_\beta \end{bmatrix} \begin{bmatrix} c_\gamma & s_\gamma & 0 \\ -s_\gamma & c_\gamma & 0 \\ 0 & 0 & 1 \end{bmatrix}$$
$$= \begin{bmatrix} c_\alpha \cdot c_\beta & c_\alpha \cdot s_\beta \cdot s_\gamma - s_\alpha \cdot c_\gamma & c_\alpha \cdot s_\beta \cdot c_\gamma + s_\alpha \cdot s_\gamma \\ s_\alpha \cdot c_\beta & s_\alpha \cdot s_\beta \cdot s_\gamma - c_\alpha \cdot c_\gamma & s_\alpha \cdot s_\beta \cdot c_\gamma + c_\alpha \cdot s_\gamma \\ -s_\beta & c_\beta \cdot s_\gamma & c_\beta \cdot c_\gamma \end{bmatrix} \quad (1)$$
$$= \begin{bmatrix} r_{11} & r_{12} & r_{13} \\ r_{21} & r_{22} & r_{23} \\ r_{31} & r_{32} & r_{33} \end{bmatrix}$$

Through the available coordinate trans- formation, we can get the translation vector of the amplifiers L_i as:

$$[L_i] = [R] \cdot [P_i] + [V] - [B_i] \quad for \quad i = 1 \sim 6 \quad (2)$$

where the displacement li as:

$$l_i = |L_i| = \sqrt{L_x^2 + L_y^2 + L_z^2} \quad for \quad i = 1 \sim 6 \quad (3)$$

IV. RESULTS AND DISCUSSION

A. Final Stage Results of simulation and experiment on a single-axis amplifier

In this research, we use the software of **SolidWorks**[@] to design and illustrate the mechanism and the software of **ANSYS**[@] to simulate the analysis of a numerical scheme with finite elements on an unstructured grid. Fig. 4 shows the deformation of each single- axis amplifier when given a force of 10 N in the numerical simulation. The line indicates the location of the amplifier before deformation and the image shows the new location after deformation. In this single-axis amplifier simulation, the number of the elements is 347,235.

To the single-axis amplifier, we suppose the longer parallel side of the trapezoid to be the fixed base (as shown in Fig. 4). The force goes with uniform distribution from the center to the input points on the flexure hinge of the inner layer. (See $B_1 \sim B_4$ in Fig. 4. B_1 and B_2 are the input points before deformation, while B_3 and B_4 are the ones after deformation.) The force increases from $1N \sim 20N$, and the deformation is calculated every time after an increase by 1N. In Fig. 4, Point C on the lower left and Point D_1, D_2 on the upper right are all output points. However, since the output point on the lower left is connected to the fixed base (see Point C in Fig. 4), its deformation is so small that it can be neglected. We only need to calculate the different values between D_1 and D_2, seeing that D_1 is the output point before deformation while D_2 is the one after deformation. By calculating the differences between B_1 and B_3, B_2 and B_4, and D_1 and D_2, we can get the displacement between the PZT and the amplifier. Nevertheless, we also calculate the linear deformation of the PZT as well as the spatial deformations of the amplifier at different forces, so that we can use them for the transformation of the six-axis stages later.
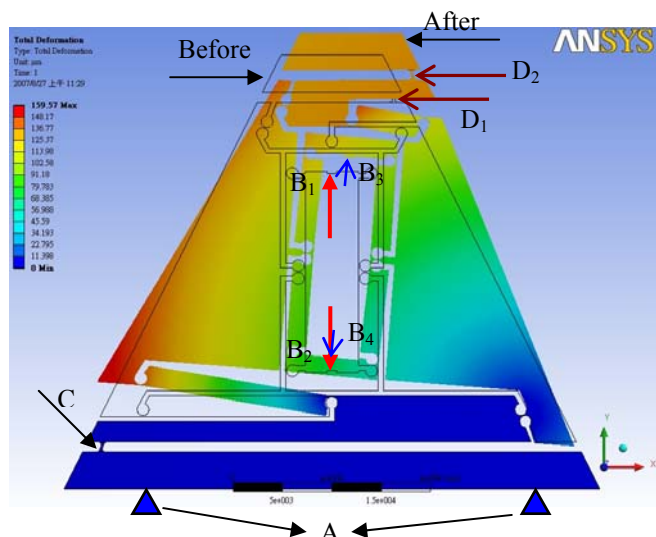
Fig. 4 The deformation at 10N in simulation

In experiment, to promote the six-axis stage accuracy, each axis of the mechanism is fabricated out of aluminum (7075), using the micromachining system, of which the rotational speed of the spindle is 40,000 rpm, and the depth of cutting of each time is 0.05mm. Fig. 5 shows the single-axis amplifier in experiment. We place into the amplifier an NEC TOKIN AE0505D16 PZT of an appropriate size that gets the PZT perfectly stuck between the contact points at both ends without causing any deformation to the amplifier to supply voltages ranging from 0 to 100 V to the input points via the center, trying to enable the amplifier to extend outwards and generate various displacements. We use an image measuring system with resolution of 1μm to repeat each of the measuring processes at different voltages three times and record the displacements of the input and the output respectively, —each time with an increase of 10 voltages, so as to calculate the amplification. However, since the lower/bottom part of the mechanism (see Point A in Fig.5) is a fixed base, the displacement of Point C near the base is too small to measure even though the force goes with uniform to

both of the contact points (see Points B_1 and B_2 in Fig. 5). Therefore, the displacement measuring end is the joining part of the flexure hinge. (See Point D in Fig. 5)

Each time, by capturing images, we measure the displacement at the upper part of the flexure hinge and calculate the relationship between the PZT and the amplifier.
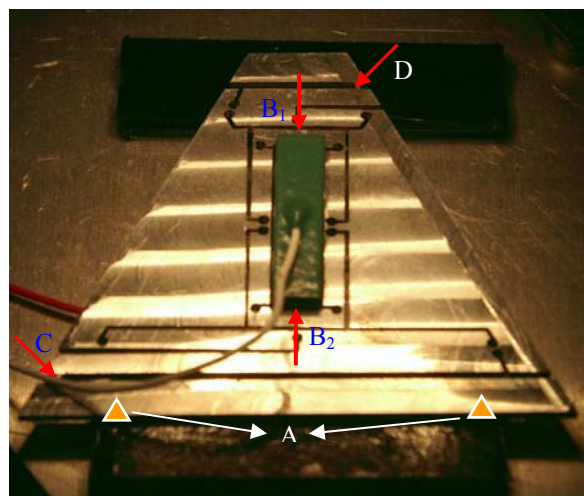
Fig. 5 A single-axis amplifier with a PZT in experiment

Fig. 6 indicates the difference between the simulation and experiment on a single-axis amplifier. The figure shows, when the input are respectively 5, 10 and 15 μm, we get the simulation deformations as 68.5, 137 and 205.5 μm, whereas we get the experiment deformations as 73, 153 and 233 μm. That is, with the same input range from 0 μm ~ 15 μm, for a single-axis amplifier, the average deformation results taken from the simulation and experiment are respectively 13.7 and 15 times as much, with an error of about 8.6%. We also see the results showing that, in the simulation, the ratio of the input forces to the input translations is 0.991387 μm/N, and that, in the experiment, the ratio of the input voltages of the PZT to the input transformation is 0.13 μm/V. Based on this, we can not only calculate the relationship of the input forces, the voltage and the elongation, but also set the parameters for the simulation and experiment of the six-axis stages.
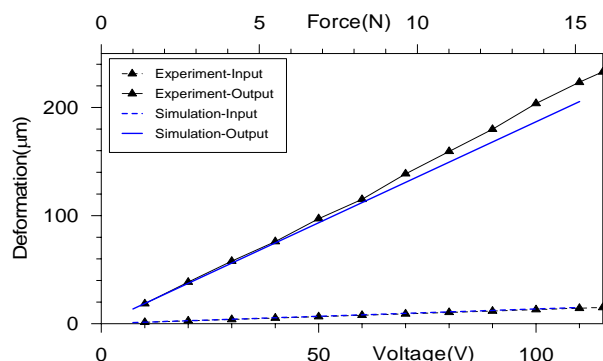
Fig.6 The results of the input and output displacements of a single-axis amplifier in simulation and experiment

B. Results of simulation and experiment on a six-axis stage

Since the six-axis micro mechanism designed in this research is to be applied to the precise micropositioning systems, such as optical fiber alignment system. With such a micro adjustment device, the maximum vertical translation, horizontal translation, tilt angle and rotational angle here are set as 50 μm, 50 μm, 0.5º, and 0.5º. Applying these parameters to Eq. (1) ~ (3), we get the calculation of the displacements of each amplifier (as shown in Table 1).

Table 1 The displacements of each amplifier

	Vertical translation 50 μm	Horizontal translation 50 μm	Tilt angle 0. 5°	Rotational angle 0. 5°
1st axis	154.8577	122.7628	123.8897	203.6697
2nd axis	154.8596	161.0910	119.4709	86.6524
3rd axis	154.8614	151.4423	140.5646	203.6726
4th axis	154.8614	151.4423	149.6574	86.6553
5th axis	154.8581	161.0899	170.9690	203.6712
6th axis	154.8577	122.7628	166.2962	86.6512

To compare their numerical solutions, analytical solutions and experiment results, we calculate the relationship from Fig.6 through interpolation and get the deformations as shown in Table 1. After that, we transform the deformations from Table 1, we obtain the resultant forces and voltages of the six-axis stages in simulation and experiment as shown in Table 2 and Table 3.

Table 2 The input forces of the six-axis stage in simulation

	Vertical translation 50 μm	Horizontal translation 50 μm	Tilt angle 0. 5°	Rotational angle 0. 5°
1st axis	11.4118	9.0466	9.1297	15.0088
2nd axis	11.4119	11.8711	8.8040	6.3856
3rd axis	11.4120	11.1601	10.3585	15.0090
4th axis	11.4120	11.1601	11.0285	6.3858
5th axis	11.4118	11.8710	12.5990	15.0089
6th axis	11.4118	9.0466	12.2547	6.3855

Table 3 The voltages of the PZT in experiment

	Vertical translation 50 μm	Horizontal translation 50 μm	Tilt angle 0. 5°	Rotational angle 0. 5°
1st axis	83.302	66.037	66.643	109.559
2nd axis	83.303	86.655	64.266	46.612
3rd axis	83.304	81.464	75.613	109.560
4th axis	83.304	81.464	80.504	46.641
5th axis	83.302	86.654	91.968	109.560
6th axis	83.302	66.037	89.455	46.612

With the input forces shown in Table 2, we then analyze the numerical simulation of the six-axis stage. We apply fine meshes to the parts where flexure hinges are located so as to perform finer analysis and medium meshes to the others. The number of meshes is totally 649,457. Of the six-axis stage, the fixed planes are the base plates (shown as the blue parts), and the measure planes are the top plates (the red parts—red

suggests where bigger displacement takes place). In simulation, each of the six input forces of the amplifiers goes with uniform distribution from the center to the contact points on the flexure hinges of the inner layers, as that of a single-axis stage does, only this time with a downward load of 1N added to each of the top plates. Fig. 7 ~ 10 show the simulated deformations of the six-axis stages respectively with varied vertical translations, horizon translations, tilt angles and rotational angles.
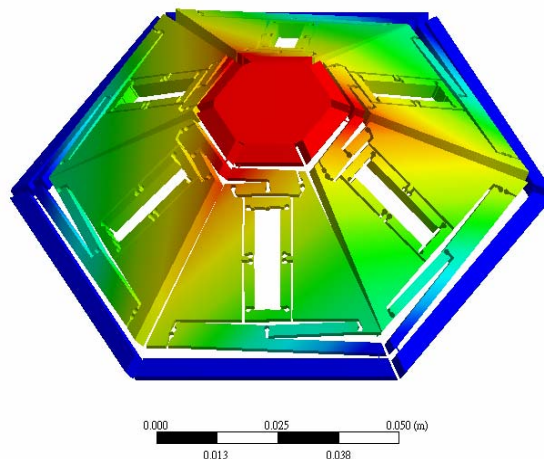
Fig. 7 Simulated deformations of the six-axis stages with varied vertical translations
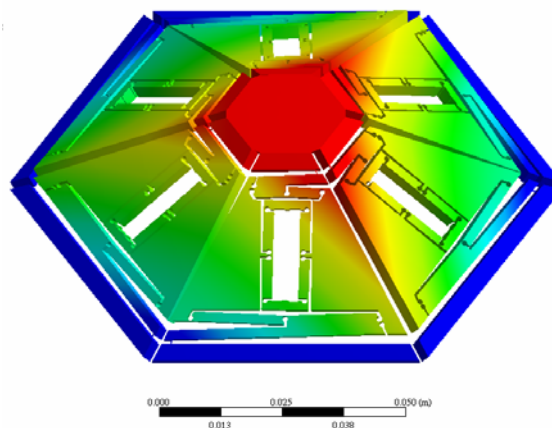
Fig. 8 Simulated deformations of the six-axis stages with varied horizon translations
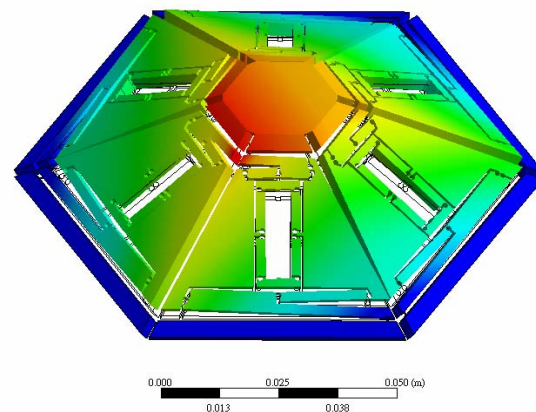
Fig. 9 Simulated deformations of the six-axis stages with varied tilt angles
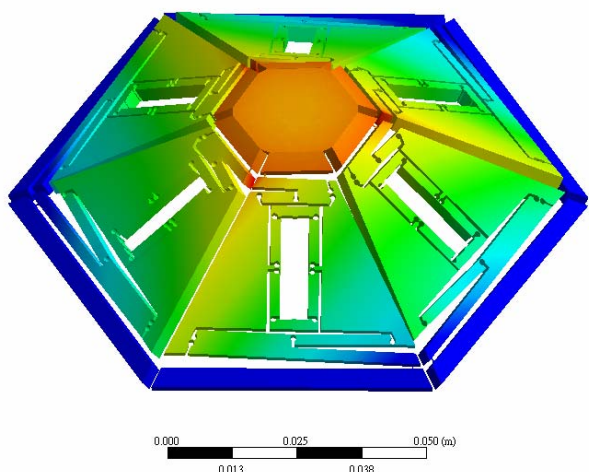
Fig. 10 simulated deformations of the six-axis stages with varied rotational angles

Fig.11 shows a six-axis mechanism in experiment. Each of the amplifiers has a PZT placed in the center; the base plate is the fixed plane and the top plate is the measure plane. When supplied with the voltages stated in Table 3, each of the PZT actuates its amplifier to extend outward so that the top plate can move to the expected position.

Fig. 11 The six-axis stages in experiment

We set a laser displacement sensor on a small coordinate measuring machines(CMM) and mark the symmetric points on the top plate of the stage. Then four different motion deformations of the stages are measured after each PZT is supplied with the voltages shown in Table 3. Table 4 shows all the expected results and the errors in simulation and experiment respectively.

Table 4 The comparison between the results and errors in simulation and experiment

	Vertical translation	Horizontal translation	Tilt angle	Rotational angle
Expected results	50 μm	50 μm	0. 5°	0. 5°
Simulated results	49.4 μm	44.8 μm	0.462°	0.45°
Simulated errors	1.2 %	10.4 %	7.6 %	10 %
Experimental results	49.28 μm	44.7 μm	0.447°	0.442°
Experimental errors	1.44 %	10.6 %	10.6 %	11.6 %

The results in both simulation and experiment show that, except that the errors in the vertical translations are under 1.5%, all of the other errors are around 10%. The reason might be that there is no restriction on the directions of displacement with a single-axis amplifier, whereas with the six-axis stages, the vertical, horizon and rotational displacements altogether need to keep the top plate horizontal, the tilt displacements need to make the top plate tilt symmetrically and no interference from the six amplifiers is allowed with one another. All these cause restriction onto the amplification and, therefore, make it hard to reach the expected range. However, when applied to manufacturing in the future, a linear scale will be built into this mechanism, and the errors in displacements can be better controlled so as to promote its precision.

V. CONCLUSION

With the mechanism of negative Poisson's ratio with flexure hinges, this research designs and fabricates a six-axis mechanism for simulation and experiment. This mechanism consists of a top plate, a base plate and six amplifiers. The top plate is a hexagon of which the diameter is 22 mm and the thickness is 3 mm, and the base plate is a hexagon of which the diameter is 95.2 mm and the thickness is 3 mm, with a distance of 21.6 mm between the two plates. Each of the amplifiers consists of three layers—two inner layers of symmetrical flexure hinges and one outer layer of non-symmetrical flexure hinge. The stage is manufactured of aluminum (7075) through micromachining.

Both of the results in simulation and experiment on a single-axis amplifier show that, with inputs from 0~15 μm, all of the amplifications are about 15 times with error under 8.6%, that the relation between the forces and the inputs is 0.991387 μm/N, and that the relation between the voltages and the inputs is 0.13 μm/V. Yet, the results in simulation and experiment on the six-axis stages show that, with the vertical translation, horizon translation, tilt angle and rotational angle respectively at 50 μm, 50 μm, 0.5º and 0.5º, only the error in vertical translation is under 1.5%, that the errors of all the other motions are about 10%, and that, with the mechanism being 100 mm x 100 mm x 30 mm, the deformation resolution is up to 15.6 nm and the rotational resolution 2.7 μrad. This indicates that the six-axis stage of this research, indeed, retains the features of high amplification and minimization. Our next target will be the application of the long travel nano stage in future.

REFERENCES

[1]   Q. Yao, J. Dong and P. M. Ferreira, "Design, analysis, fabrication and
      testing of a parallel-kinematic micropositioning XY stage," Mechine
      tools and manufacture, Vol. 47, pp. 946-961, 2007.
[2]   W. J. Kim, S. Verma and H. Shakir, "Design and precision construction
      of novel magnetic-levitation- based multi-axis nanoscale positioning
      systems", precision Engineering, Vol. 31, pp. 337-350, 2007.
[3]   Y. Wu and Z. Zhou, "An XYθ mechanism actuated by one actuator",
      Mechanism and Machine Theory, Vol. 39, pp. 1101-1110, 2004.
[4]   H. H. Pham and I. Chen, "workspace and static analyses of 2-DOF
      flexure parallel mechanism", Seventh International Conference on
      Control, Automation, Robotics and Vision, pp. 968-973, 2002.
[5]   C. L. Chu and S. H. Fan, "A novel long-travel piezoelectric-driven
      linear nanopositioning stage", Precision Engineering, Vol. 30, pp.
      85-95, 2006.
[6]   W. Gao, S. Dejima, H. Yanai, K. Katakura, S. Kiyono and Y. Tomita,
      "A surface motor-driven planar motion stage integrated with an XYθZ
      surface encoder for precision positioning", Precision Engineering, Vol.
      28, pp. 329-337, 2004.
[7]   Stewart, D., A Platform with Six Degrees - of - Freedom, Proc. Inst.
      Mech. Eng., Vol. 180, No. 1, pp. 371-386, 1965.
[8]   Sigmund, O., Tailoring materials with prescribed elasticproperties,
      Mechanics of Materials Vol. 20, pp. 351- 368, 1995.
[9]   Trease, B. P., Moon, Y. M. and Kota, S. Design of large-Displacement
      Compliant Joints, Trans. of the ASME, Vol. 127, pp.788-798, 2005.
[10] Lin, K. H., Hu,Y. H. Huang, C. M. and Fu, C. J, Design and Numerical
      Simulation of Piezoelectric Micro-Platform, Journal of Ching-Yun
      University, Vol. 26, No. 1, pp. 25-34, 2006.
[11] Sigmund, O., Tailoring materials with prescribed elasticproperties,
      Mechanics of Materials Vol. 20, pp. 351- 368, 1995.
[12] Gao, P and Swei, S. M., A six-degree-of -freedom micro-manipulator
      based on piezoelectric translators, Nanotechnology, Vol. 10, pp.
      447-452, 1999.
[13] W.-K. Chen, Linear Networks and Systems (Book style).Belmont, CA:
      Wadsworth, 1993, pp. 123–135.